Design of Polyazamacrocyclic Gd^{3+} Theranostic Agent Combining MRI and Two-Photon PDT

Laura Abad Galán,‡[a] Nadège Hamon,‡[b] Christophe Nguyen,[c] Enikő Tóth,[d] János Kiss,[e] Jonathan Mendy,[b] Kamel Hadj-Kaddour,[c] Mélanie Onofre,[c] György Trencsényi,[f] Cyrille Monnereau,[a] Maryline Beyler,[b] Gyula Tircsó,[d] Magali Gary-Bobo,[c,*] Olivier Maury,[a,*] Raphaël Tripier[b,*]

Abstract. New "all-in-one" theranostic systems, combining a magnetic resonance imaging (MRI) contrast agent with a biphotonic photodynamic therapy (2P-PDT) photosensitiser generating cytotoxic singlet oxygen, were envisaged and synthesised. They are based on azamacrocycles, regiospecifically functionalised by two-photon PDT π-conjugated dibromobenzene-picolinate photosensitisers and acetate, able to complex gadolinium(III) and allow an MRI signal. Our approach was to use two different macrocyclic platforms, tacn and pyclen, for modulating simultaneously the structures, properties and solubility of the complexes. Photophysical properties of the ligands and their gadolinium(III) complexes were fully investigated. The Gd^{3+}-pyclen derivative showed the best water solubility and the greatest value of singlet oxygen generation of the series with ϕ_Δ = 0.53 enabling in vitro studies. The biological PDT activity under mono and biphotonic excitation was evaluated in human breast cancer cells (MCF-7). While a very low dark toxicity was observed, an almost total cell death was induced after only 3 successive irradiations of 1.57 sec. Finally, its relaxivity was measured in a DMSO/H_2O solvents mixture with r_{1p} = 11.21 and r_{2p} = 24.60 $mM^{-1}s^{-1}$ at 3.0 T and T_1- and T_2-weighted phantom MR images were obtained highlighting a first generation of "all-in-one" PDT/MRI theranostic agents.

Introduction

The term *theranostic* is the portmanteau word of *therapy* and *diagnostic*; it is an emerging field of research that aims to combine within the same bioprobe, the detection and treatment of a target disease. On the one hand, the imaging methodology can for example rely on fluorescence microscopy, magnetic resonance imaging (MRI) or radioisotope imaging (positron emission tomography: PET, single-photon emission computed tomography: SPECT).[1] On the other hand, the therapeutic function can be achieved by a local delivery of active chemicals, radioactivity or singlet oxygen reactive species as in PDT (PDT: photodynamic therapy).[2] To date, most of the bioprobes designed for theranostic applications are surface modified nano-sised objects[3-6] and there has been comparatively less focus on molecular bioprobes.[7-10] In most reported molecular systems, theranostic properties arise from the combination of two individual functionalities covalently connected into one single object[8, 11-15] with seldom report of "all-in-one" molecular bioprobe.[16,17] Most of the theranostic bioprobes contains transition metals or f-elements for their specific properties and, so far, Gd^{3+}-based MRI is particularly concerned.[18,19] In this specific area, the commercially available cyclen-based ligand, dota (1,4,7,10-tetraazacyclododecane-1,4,7,10-tetraacetic acid), which is a very strong lanthanide(III) chelator, is nowadays universally used as a Gd^{3+} contrast agent (CA) in MRI.[20, 21] However, with the aim to improve the sensitivity of these CAs, alternative macrocycles such as tacn (1,4,7-triazacyclononane)[22-24] and in less explored cyclam (1,4,8,11-tetraazacyclotetradecane)[25] or pyclen (1,4,7,10-tetraaza-2,6-pyridinophane), an often overlooked azamacrocyclic platform,[26-28] have also been studied during these last decades. Besides showing improved performances in terms of metal complexation over cyclen-based chelators, they also allow the easier introduction of π-conjugated antennas to permit optical modalities. We, among others, have used such chemical modifications to design cyclen,[29,30] cyclam[31] but, especially, tacn[32-35] and pyclen[36,37] frameworks functionalised by picolinate functions for the development of both gadolinium(III) CA (GdCA) and lanthanide(III) luminescent bioprobes (LLB). More recently we presented a lanthanide(III) (Yb^{3+} and Gd^{3+}) two-photon photosensitizer for PDT[38] that opened the way for the design of an "all-in-one" probe combining MRI and PDT.

Indeed, in terms of therapeutic development, PDT is nowadays considered as a frontline alternative in clinical cancer treatment.[39, 40] As said, it consists in the local generation of cytotoxic singlet oxygen

[a] *Univ Lyon, ENS de Lyon, CNRS UMR 5182, Université Claude Bernard Lyon 1, Laboratoire de Chimie de l'ENS de Lyon, F-69342 Lyon, France ; olivier.maury@ens-lyon.fr*
[b] *Univ Brest, UMR-CNRS 6521 CEMCA, UFR des Sciences et Techniques, 6 avenue Victor le Gorgeu, C.S. 93837, 29238, Brest, Cedex 3, France ; raphael.tripier@univ-brest.fr*
[c] *IBMM, Univ Montpellier, CNRS, ENSCM, F-34000 Montpellier, France; magali.gary-bobo@inserm.fr*
[d] *University of Debrecen, Department of Physical Chemistry, Debrecen, Egyetem tér 1, H-4032, Hungary*
[e] *University of Debrecen, Clinical Centre, Department of Medical Imaging, Radiology, Debrecen, Nagyerdei Krt. 98, H-4032, Hungary*
[f] *University of Debrecen, Faculty of Medicine, Medical Imaging Department, Division of Nuclear Medicine, Debrecen, Nagyerdei Krt. 98, H-4032, Hungary*

Electronic Supplementary Information (ESI) available: [Ligands and complexes synthesis and characterisation; Photophysical and relaxivity measurements].

‡These authors contributed equally to the work.

by a photosensitizer under light irradiation, offering a fine control over the site selectivity of the therapeutic effect. In this context, porphyrin based sensitizers nowadays of widespread use for treatments of melanoma (Forscan) or macular degeneration (Visudyne) for example.[41] However, monophotonic excitation of the latter takes place in the visible part of the electromagnetic spectrum (ca 600-650 nm), where the absorption and scattering of visible light by tissues restricts the use of one photon-PDT to surface treatment of the targeted sites. Comparatively, two-photon absorption permits to work in the near infra-red biological transparency window and to benefit from the high spatial resolution of the excitation.[42, 43] This has fueled the development of new 2P-PDT sensitizers since the early 2000's.[39, 40] In this context, we and others developed dibrominated 2P-PDT sensitizers,[44-46] and designed complex [Gd**L1**],[38] a **no3pa**-Gd^{3+} derivative (Figure 1a; coordination number, CN = 9, q = 0). Combination of the effect of bromine substituents and coordination of the ligand with Gd^{3+} led to a synergistic effect on the singlet oxygen generation efficiency of the resulting complex (ϕ_Δ = 0.8 in chloroform).[47-51] The resulting complex [Gd**L1**] also displayed large 2PA cross-section (540 GM), and we showed that micellar suspensions of the latter in pluronic was efficient in generating cancer cell death under 2P-activation.[38]

Based on this background, we designed two new original MRI/PDT theranostic agents, complexes [Gd**L2**(H_2O)] and [Gd**L3**(H_2O)] (CN = 9, q = 1), using either a tacn ligand featuring two PDT-antennas and one acetate pendant moiety or a pyclen one, with one PDT sensitiser and two acetate arms arranged in a dissymmetric manner (Figure 1b). Those parent ligands, **no1a2pa**[22] and **pc2a1pa**[28] respectively, previously showed to form outstanding complexes with gadolinium(III) (Figure 1),[22, 28] with an available coordination site for water, that could be exploited for MRI applications. Furthermore, to remediate the low solubility of [Gd**L1**] in water, substitution of the picolinate moieties of the **no1a2pa** and **pc2a1pa** frameworks by two-photon PDT (2P-PDT) antennas incorporating polyoxyethylene glycol end-groups was envisaged rather than hexyl termination, to afford as much as possible the required water solubility for biological application. After detailed photophysical studies, the best suited compound was involved in a series of biological experiments. Biocompatibility of the molecule was investigated by measuring its dark cytotoxicity on human breast cancer cells (MCF-7). Then, the phototoxicity was determined under 1P and 2P-excitation to evaluate its phototherapeutic efficiency. Finally, the efficacy of the Gd^{3+} complex as potential MRI contrast agent (MRI-CA) candidate was determined by measuring its magnetic properties and calculating its relaxivity, and T_1- and T_2-weighted phantom MR images at different concentrations were recorded by using clinical MRI scanners.

Results and discussion

Synthesis. Chromophore **7** was synthesised in four steps from the PEGylated (polyoxyethylene glycol) *para*-ethynylbenzenamine **1** following procedures similar to those reported for analogous derivatives as summarised in Scheme 1.[38] A first Sonogashira coupling between compound **1** and iodinated-aryl derivatives **2** in the presence of $Pd(PPh_3)_2Cl_2$ and CuI led to compound **3**. Deprotection of the silylated alkyne was performed with potassium carbonate in THF/MeOH and the resulting alkyne **4** was engaged in a second Sonogashira coupling with the iodo-picolinate methyl ester **5** to afford compound **6** in quantitative yield. Mesylation of the latter was performed under usual conditions and led quantitatively to the mesylated antenna **7**. Once the chromophoric arm was synthesised, the alkylation of tacn was performed with two equivalents of the mesylated bidendate derivative **7**, yielding compound **8** in a

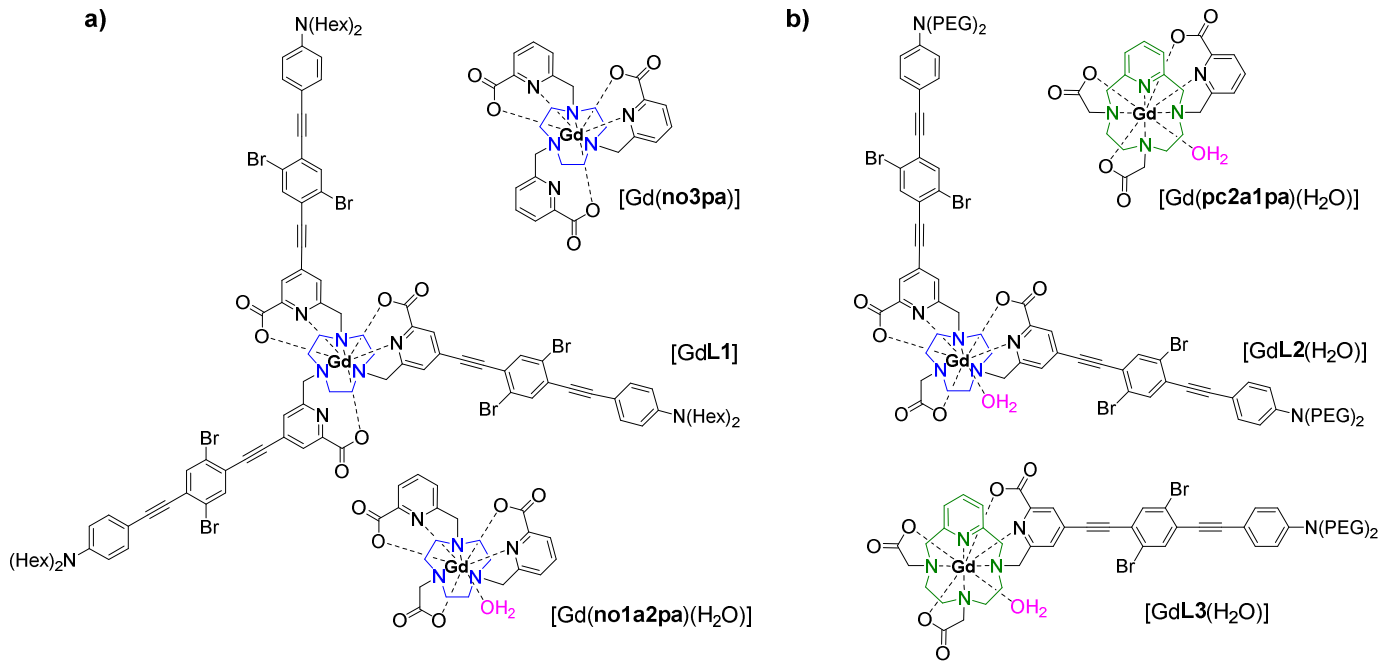

Figure 1. Representation of previously studied derivatives (a) and the three Gd^{3+} complexes studied in this report (b).

moderate 55 % yield. The third nitrogen was later linked to an acetate group to afford compound **9** (Scheme 2) in 48% yield. The strategy of synthesis for the pyclen derivative was slightly modified in comparison to the tacn analogue and consisted in the late introduction of the chromophoric arm **7** on one amine of the pyclen skeleton (Scheme 2). We then took advantage of our recently described regiofunctionalised synthesis of pyclen **10**, where two adjacent amine groups are bearing acetate arms thanks to a preliminary protection of the macrocycle with the Alloc group.[52]

Alkylation of macrocycle **10** with one equivalent of the mesylated bidendate chromophoric arm **7** was performed following previously reported procedures to afford compound **11** in 60% yield.[37]

Finally, complexation was achieved in a one-pot strategy that started by saponification of the ester groups of **9** or **11** prior to the addition of the gadolinium salt ($GdCl_3.6H_2O$) at pH = 6, resulting in compounds [Gd**L2**(H_2O)] and [Gd**L3**(H_2O)], respectively (Scheme 2). Following this approach, the two eight-coordinated complexes could be obtained, leaving the ninth position available to further coordinate a molecule

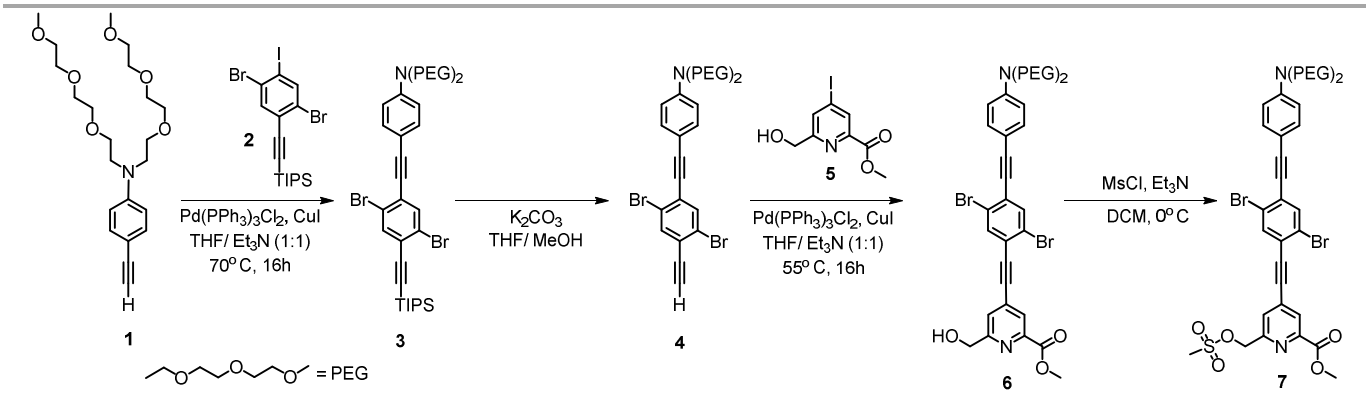

Scheme 1. Synthethic procedure followed for the synthesis of the chromophoric arm **7**.

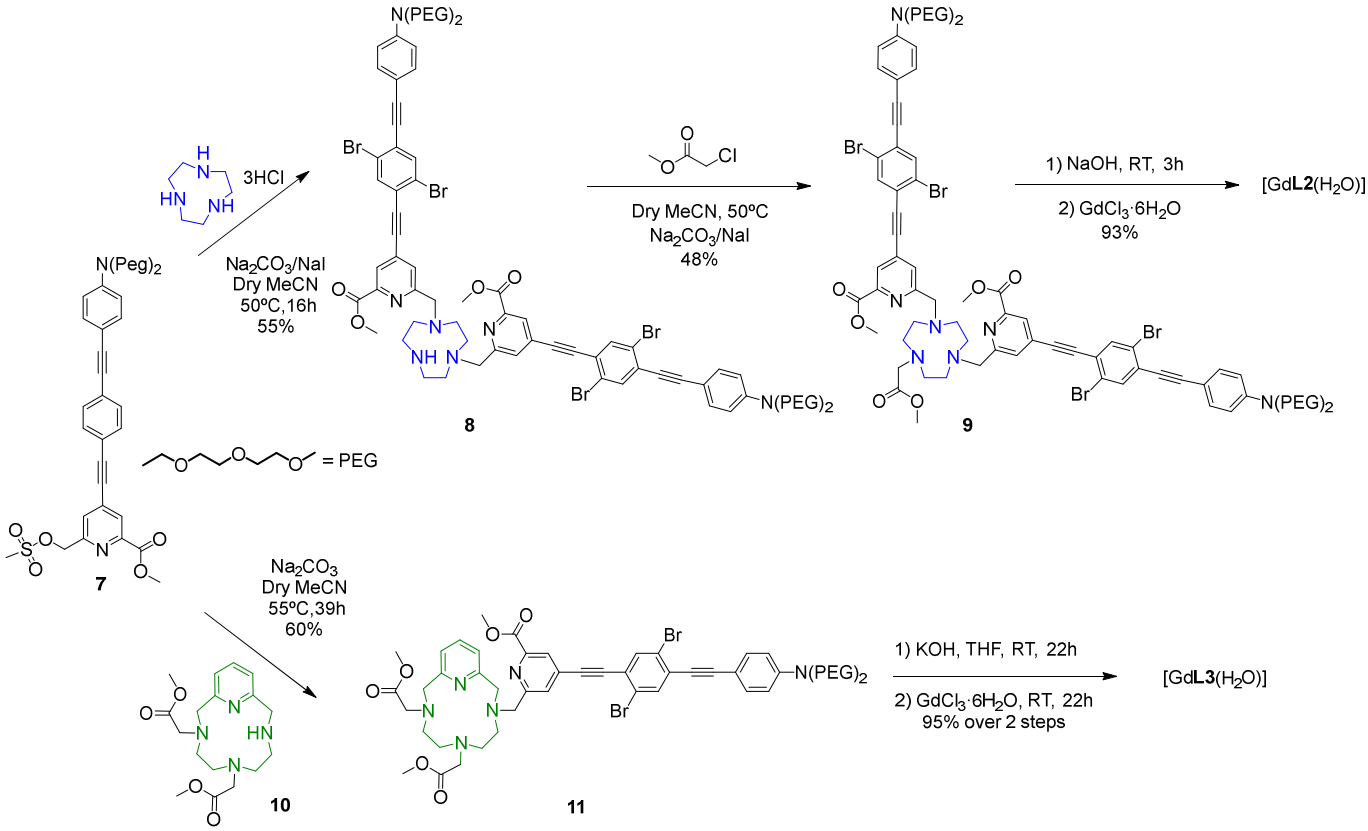

Scheme 2. Synthetic procedures for the preparation of Gd^{3+} complexes of [Gd**L2**(H_2O)] and [Gd**L3**(H_2O)].

Table 1. Main photophysical data for **9**, **11** and their Gd^{3+} complexes [Gd**L2**(H_2O)] and [Gd**L3**(H_2O)].

	Solv.	λ_{abs} [a]	ε [b]	λ_{em} [a]	Φ_F [c]	Φ_Δ [d]
9	DCM	302, 415	31500	596	0.05	0
	H_2O	310, 412	-	635	-	-
[Gd**L2**(H_2O)]	DCM	297, 420	53000	620	0.02	0.38
	H_2O	309, 410	-	620	-	-
11	$CHCl_3$	310, 415	22500	577	0.04	0.46
	H_2O	310, 412		635	<0.01	0.15
[Gd**L3**(H_2O)]	$CHCl_3$	310, 414	24000	560	0.01	0.53
	H_2O	310, 415		630	<0.01	0.18

[a] λ_{abs} and λ_{em} expressed in nm ; [b] ε expressed in $Lmol^{-1}cm^{-1}$; [c] luminescence quantum yield is measured in the visible region considering only the residual emission of the ligand-centred transition with coumarin 153 in MeOH used as reference (λ_{ex} = 400 nm, ϕ_{ref} = 45 %). [d] Phenalenone in DCM used as a reference compound (ϕ_Δ = 95 %).

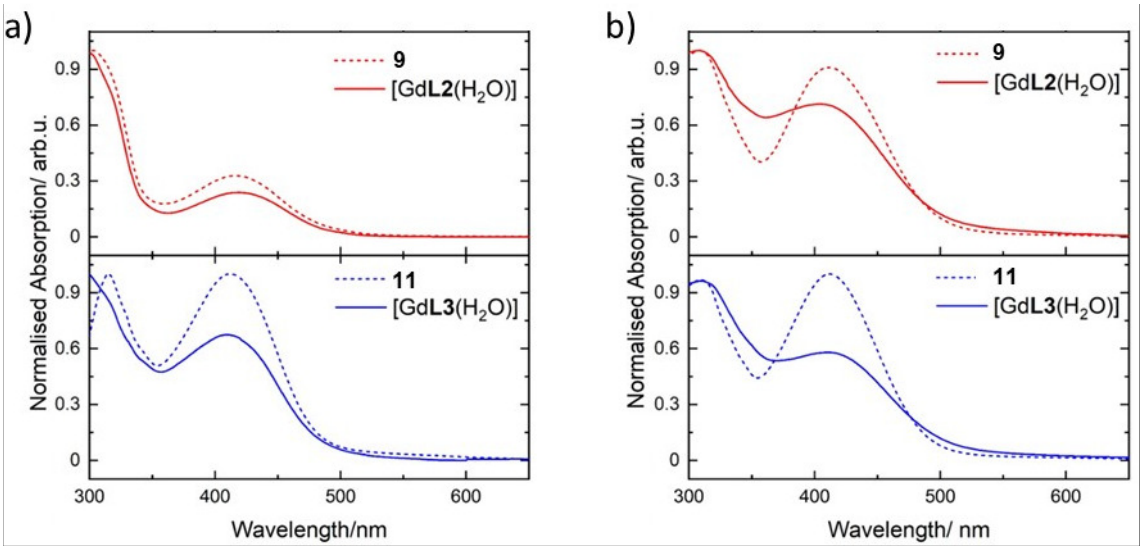

Figure 2. Normalised absorption spectra of ester ligand **9** (red full trace) and its corresponding [Gd**L2**(H_2O)] complex (red dashed trace); and ester ligand **11** (blue full trace) and its corresponding [Gd**L3**(H_2O)] complex (blue dashed trace) in dichloromethane (a) and water (b) solutions at room temperature.

of water, as previously proven in the literature.[22] Complete characterization of the previously cited compounds (NMR, HRMS, analytic HPLC) is reported in the supporting information (Figures S1 to S11).

Photophysics. The photophysical properties of the gadolinium(III) complexes [Gd**L2**(H_2O)] and [Gd**L3**(H_2O)] and the ester derivatives **9** and **11**, including absorption, emission, fluorescence quantum yield and singlet oxygen generation, were studied in both diluted dichloromethane and water solutions (Table 1 and supporting information, Figures S12 to S21 and Table S1). In spite of the introduction of PEGylated end-substituents, a poor solubility of the tacn complex [Gd**L2**(H_2O)] in water was observed. In contrast, the solubility of [Gd**L3**(H_2O)] in water turned out to be significantly impoved, probably because of the presence of only one hydrophobic PDT arm. By comparison of the absorption spectra of these compounds with similar previously studied chromophores,[38] the lowest energy band, found in both solvents around 400 nm, can be assigned to the characteristic charge transfer (CT) transition from the electron-donating dialkylamino group to the electron-withdrawing picolinate (Figure 2). On the other hand, the higher energy band (~300 nm) corresponds to a π-π* transition, localised on the central

part of the scaffold.[38] Complexation has only a minor effect on the localization and features of the absorption bands. The molar absorptivity of the tacn ester ligand **9** was of ~ 35000 $Lmol^{-1}cm^{-1}$, while its gadolinium(III) complex showed an enhancement with up to ~ 50000 $Lmol^{-1}cm^{-1}$. As expected, this value is reduced in comparison to the previously reported complex [Gd**L1**] containing three analogous antennas,[38] with an absorbance of the ester ligand and complex resulting essentially from the additive contribution of the anchored arms, and being thus proportional to their number. Therefore, it is expected that **11** and its complex [Gd**L3**(H_2O)] present lower molar absorptivity, which is consistent with the experimental values of 22500 $Lmol^{-1}cm^{-1}$ and 25000 $Lmol^{-1}cm^{-1}$, respectively. Just like the molar extinction coefficient, the two-photon absorption cross-section is known to be an additive values depending only on the nature of the antenna chromophore.[31, 36] Keeping in mind that the parent antenna ligand **L1,** featuring three brominated antennas, present a two-photon cross-section of 540 GM at 810 nm,[38] it can be anticipated that **9** and **11** present an estimated cross-section of *ca* 360 GM and 180 GM, respectively (2/3 and 1/3 of **L1**, respectively).
All ligands present a similar typical broad CT ligand emission band centred around 580 nm in the case of dichloromethane and above 600 nm in water, associated with the brominated antenna, which undergoes a minor shift upon coordination (Figure S16). The fluorescence quantum yield associated to this transition band turned out quite low for both **9** and **11**, in good agreement with a favoured ISC process due to heavy atom effect (as previously seen for **L1**). For the corresponding complexes [Gd**L2**(H_2O)] and [Gd**L3**(H_2O)], this emission band is nearly supressed ($\Phi_F \leq 0.01$) as an indication of a possible additional ISC enhancement upon incorporation of Gd^{3+}, which acts as a heavy atom, and/or increased non-radiative decays.

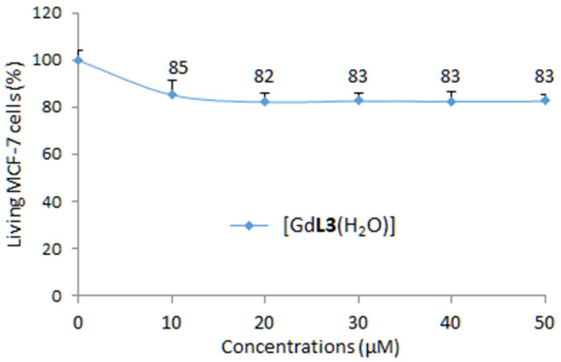

Figure 3. Cytotoxic study performed on MCF-7 cells incubated with increasing concentrations of [Gd**L3**(H_2O)] (0 to 50 µM) for 72 h in the dark.

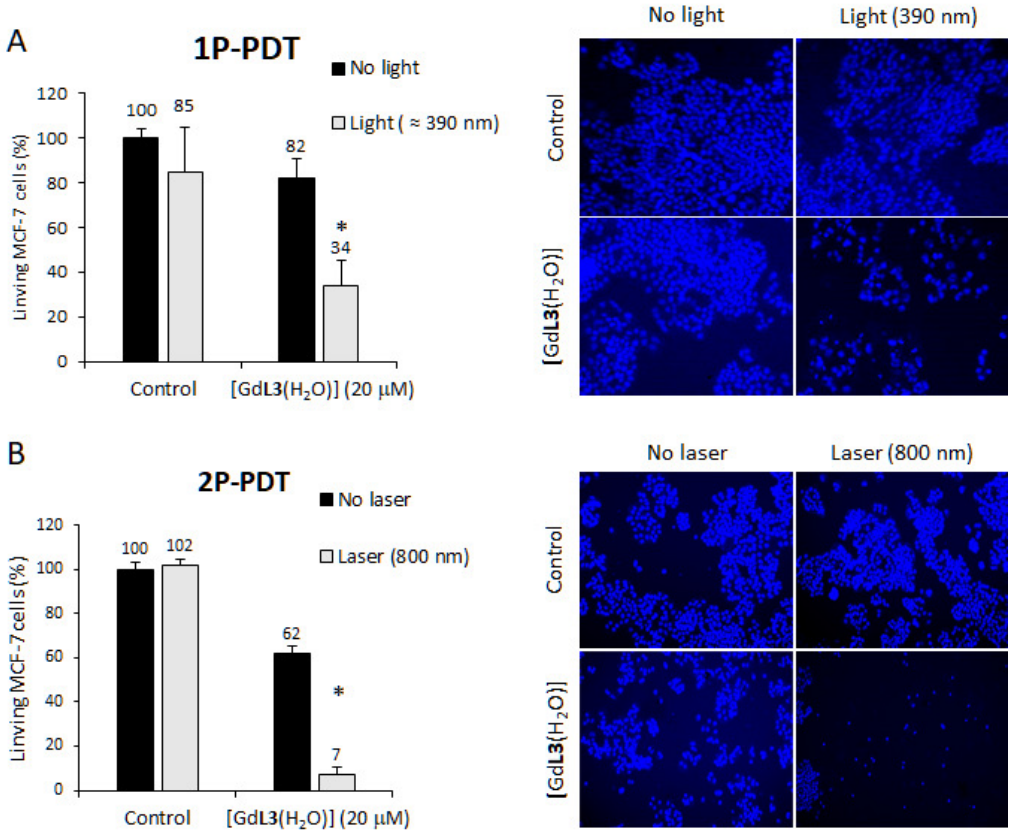

Figure 4. For PDT experiments, MCF-7 cells were incubated with 20 µM [Gd**L3**(H_2O)] for 24 h. (A) 1P-PDT: cells were excited with a mercury lamp at λ_{exc} ≈ 390 nm, 10 min. Control correspond to non-incubated cells in the absence or presence of light irradiation. (B) 2P-PDT experiment: cells were irradiated with a pulsed laser by 3 scans of 1.57 sec at 800 nm (max power laser input 3W). Cell survival measurements were done by Hoechst staining and cell counting. Bar graphs are mean values ± standard deviation from 3 experiments. *$p \leq 0.05$ for complexes: no laser vs laser (Student *t*-test). Pictures of fluorescent nuclei are selected areas representative of the entire well, cells were stained with Hoechst dye under UV 1P-irradiation.

The generation of singlet oxygen, as key requirement for PDT, was therefore studied in both media. In the case of dichloromethane, the formation of singlet oxygen could be followed by direct observation of its phosphorescence band at 1270 nm. In water, where singlet oxygen lifetime is dramatically reduced so that the observation of its phosphorescence band is not feasible, this study was performed with an oxygen scavenger. In the present case, the chosen scavenger was dipropionic acid anthracene (DPAA) following a well-established protocol already reported in previous articles.[38, 53]

While ester ligand **9** (despite of the presence of bromine substituents) does not present measurable singlet oxygen generation in DCM or water, incorporation of Gd^{3+} provides a significant enhancement of this parameter. [Gd**L2**(H_2O)] presents indeed a singlet oxygen generation quantum yields (ϕ_Δ) of 0.38, in DCM, while its low solubility precludes measurements in water. In contrast, compound **11** alone presents a significant singlet oxygen sensitization efficiency (ϕ_Δ = 0.46), which is further improved upon Gd^{3+} complexation (= 0.53). The results showed a higher singlet oxygen generation for the complexes than their corresponding ester ligands in both media, in agreement with the reduced fluorescence quantum yield, suggesting an enhanced ISC due to heavy atom coordination.[47-49, 54] Compared to [Gd**L1**] (ϕ_Δ = 0.80 in DCM) the lower photosensitising properties of [Gd**L2**(H_2O)] can be tentatively explained by the presence of coordinated water molecule favoring additional non-radiative pathways and probably also the PEGylated chains. Both complexes exhibit therefore all the prerequisites to be a MRI/PDT Gd^{3+}-based theranostic probe, namely an open coordination sphere with one water molecule and the ability to generate singlet oxygen under 1P- or 2P-irradiation. Unfortunately, the tacn complex [Gd**L2**(H_2O)] shows a rather poor solubility in water not compatible with biological and MRI experiences where 10^{-4} and 10^{-3} M concentrations are required and was then discarded in favor of the pyclen derivative [Gd**L3**(H_2O)], which was selected for the application studies.

Biological studies in cells. First, the biocompatibility of [Gd**L3**(H_2O)] was verified on human breast cancer cells (MCF-7) in the dark. To this end, cells were incubated 72 h with increasing concentrations of the Gd-complex. As this complex was initially dispersed in DMSO; the cell death induced by DMSO itself was measured and taken into account to describe only the cell death induced by Gd-complex. In Figure 3, we can observe that the pyclen complex [Gd**L3**(H_2O)] showed toxicity at the limit of significance with 17% of cell death at 50 µM. Then, cells were incubated during 24 h with 20 µM of [Gd**L3**(H_2O)] and submitted to one-photon (1P) excitation (λ_{exc} ≈ 390 nm) or two-photon (2P) excitation (λ_{exc} = 800 nm) and their photoactivity was reported in Figures 4A and 4B, respectively. Interestingly, the monophotonic excitation (λ_{exc} ≈ 390 nm, 10 min) of cells incubated with [Gd**L3**(H_2O)] induced 66% of mortality, a value significantly higher than the control experiment carried out either in presence of [Gd**L3**(H_2O)] in the dark (cell death was only 18%) or upon photoactivation in the absence of the complex (cell death was 15 %). Finally, under two-photon excitation (2PE) [Gd**L3**(H_2O)] induced an almost total cell death after only 3 successive irradiations of 1.57 sec, and therefore less than 5 sec of pulsed laser excitation. Here again, cell death obtained under 2PE in the absence of [Gd**L3**(H_2O)] did not lead to any measurable cell death. All together, these results obtained on human cancer cell line demonstrated the biomedical potential of such Gd^{3+}-complex for PDT under 1P or 2P excitation with an enhanced efficiency under 2PE.

Relaxivity and MRI performance. Thanks to the presence of a water molecule in the ionosphere of the Gd^{3+} complexes, considering the positive results in terms of singlet oxygen generation, the most water soluble [Gd**L3**(H2O)] was evaluated for its relaxation properties and therefore its potential as a first PDT/MRI theranostic agent. As said in introduction, efficacy of a potential MRI-CA candidate is determined by its magnetic properties described by its r_{1p} and r_{2p} relaxivities (relaxivity of a paramagnetic substance is the relaxation rate enhancement caused by the presence of 1 mM paramagnetic species vs. the diamagnetic contribution). The parent [Gd(**pc2a1pa**)(H_2O)] complex possesses relaxivity (r_{1p}) of 4.95 $mM^{-1}s^{-1}$ determined at 0.47 T and 25°C which is typical for a small Gd^{3+} complex containing a metal coordinated water molecule (Table 2).[28]

Table 2. Relaxivity ($mM^{-1}s^{-1}$) of the Gd^{3+} ion and [Gd(**pc2a1pa**)(H_2O)] and [Gd**L3**(H_2O)] complexes measured in pure H_2O and 32% (v/v %) DMSO/H_2O solvents mixture (I=0.15 M NaCl and for the complexes the pH was set to 7.4 by HEPES buffer).

	Gd^{3+}, [a]	Gd^{3+}, [b]	[Gd(**pc2a1pa**)(H_2O)] [b]	[Gd**L3**(H_2O)] [b]
r_{1p}	11.23	20.42	9.34[c]	11.60
r_{2p}	13.12	22.54	10.73	16.05

[a] in pure water; [b] in 32% DMSO/H_2O mixture; [c]4.95 $mM^{-1}s^{-1}$ determined at 0.47 T and 25°C from [28].

The increase in molecular mass as a result of the substitution of the picolinate pendant arm by the PEGylated chromophore derivative is expected to affect positively the relaxation properties of the resulting Gd^{3+} complex because the tumbling rate of the molecules is known to decrease with increasing molecular mass/size, which in turn results in relaxivity increase. However, even though solubility of [Gd**L3**(H_2O)] complex in pure water was the highest between both complexes, it was found insufficient in regard with the *ca* mM concentrations required for the targeted experiments (Figures S22 to S24 and Table S2 in supporting information). Therefore, its relaxation properties were determined by measuring the spin-lattice (T_1) and spin-spin relaxation times (T_2) of the water protons for the solutions of the complex prepared in DMSO/H_2O solvent mixture. The use of solvent mixtures (organic/water) being also know to affect the relaxivity[53] (effect of the viscosity on the rotational correlation time τ_r and electron relaxation time τ_s), the relaxivity of the Gd^{3+} ion ($GdCl_3$ salt) and that of the parent [Gd(**pc2a1pa**)(H_2O)] complex were also evaluated in the same solvent mixture. As it is seen in Figure S22 (supporting information) by increasing the molar fraction of the DMSO in H_2O, the relaxivity of the Gd^{3+} ion also increases. The [Gd**L3**(H_2O)] complex could be dissolved by using 30% (v/v %) DMSO/H_2O solvent mixture allowing us to prepare a [Gd**L3**(H_2O)] stock solution of 0.78 mM concentration. The composition of the

solvent was kept constant in further studies at 32% (v/v %) of DMSO in order to prevent the precipitation of the complex in the samples used in relaxivity and MRI measurements. As it is seen in Table 2, under these conditions the Gd^{3+} ion has a relaxivity of r_{1p}=20.42 and r_{2p}=22.54 $mM^{-1}s^{-1}$ (1.41 T and 25 °C) whereas in pure water it displays considerably smaller (r_{1p}=11.23 and r_{2p}=13.12 $mM^{-1}s^{-1}$) relaxation enhancement.

The relaxivity of the [Gd**L3**(H_2O)] complex was calculated using the relaxation times and concentrations at 1.41, 1.5 and 3.0 T field strengths (the latter two fields correspond to the field used in clinical MRI scanners) and was found to be r_{1p}=11.60, 9.96 and 11.21 $mM^{-1}s^{-1}$, respectively whereas the r_{2p} values change in the following order: 16.05, 11.21 and 24.60 $mM^{-1}s^{-1}$. While these values are, as anticipated, smaller than those measured for the Gd^{3+} ion in the same solvent mixture, they are however significantly larger than those observed for the parent [Gd(**pc2a1pa**)(H_2O)] complex, due to the presence of the two-photon PDT photosensitiser (r_{1p}=9.34 and r_{2p}=10.74 $mM^{-1}s^{-1}$ at 1.41 T and 25 °C). Based on these data, the observed (25% in r_{1p} and nearly 50% in terms of r_{2p}) increase in relaxivity of [Gd**L3**(H_2O)] when using DMSO/H_2O mixture can be attributed to the increased molecular mass of the complex and its slower tumbling/rotation in solution.

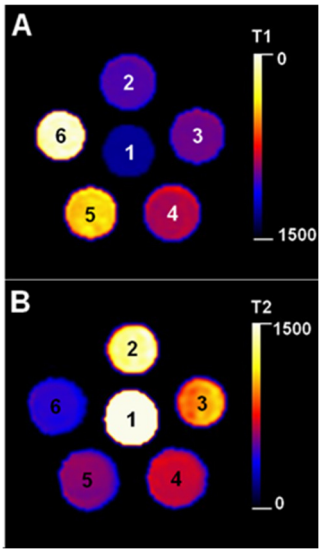

Figure 5. Representative T_1- (A) and T_2-weighted (B) MR (3T) images of [Gd**L3**(H_2O)] samples at different concentrations: 1. pH=7.4 HEPES buffer only; 2. 0.087; 3. 0,116 mM; 4. 0,174 mM; 5. 0,347 mM and 6: 0,5790 mM [Gd**L3**(H_2O)] (I=0.15 M NaCl, pH=7.4 set by HEPES buffer). The T_1 and T_2 relaxation times are shown on msec scale.

To evaluate the efficiency of the [Gd**L3**(H_2O)] complex as T_1 or T_2 shortening agent, T_1- and T_2-weighted phantom MR images of the complex at five different concentrations (0.087, 0.116, 0.174, 0.347 and 0.579 mM) were recorded at 1.5 and 3.0 T field strengths by using clinical MRI scanners. The qualitative analysis of the MR images confirmed that the image intensities observed in the presence of [Gd**L3**(H_2O)] increase with increasing concentrations and the differences between the concentrations of the samples can be visualised based on the differences in signal intensity (Figure 5). Owing to the high relaxivity of the [Gd**L5**(H_2O)] chelate, even small changes in the concentration of the agent were reliably visualised both on T_1- and T_2-weighted images.

Conclusions

In this paper, we reported the investigation of metal-based imaging and therapy probes. For the first time to our knowledge, the two modalities are set within the same molecule thanks to the dual capability of azamacrocycles to be decorated with functional groups and to coordinate metals of interest. Herein, two potential theranostic probes, built on a tacn or pyclen macrocyclic platform, were functionalised with an adequate number of acetate and picolinate-modified PDT arms to leave, after complexation of gadolinium(III), a coordination site available for water binding. The multi-step synthesis and characterization of the PDT arm, the ligands and their Gd^{3+} complexes are fully described. The photophysical studies of the monohydrated chelates in organic and aqueous solutions underline the heavy atom effect of bromide groups but also gadolinium(III) that remarkably favors the generation of cytotoxic singlet oxygen under two-photon excitation.

The biocompatibility and specific PDT activity of the most soluble complex [Gd**L3**(H_2O)] was evaluated. Under two-photon excitation, nearly quantitative death of human cancer cells was achieved after 3 successive irradiations of 1.57 s. Finally, owing its high relaxivity the pyclen derivative [Gd**L3**(H_2O)] could be used for MRI experiments, even if, despite the presence of solubilizing PEGylated side chains, the complexes show limited solubility in water. In a DMSO/water solvent mixture, an increase of relaxivity, compared to its parent complex [Gd(**pc2a1pa)**(H_2O)] was observed and attributed to the increase of molecular weight after addition of the two-photon PDT moieties. T_1- and T_2-weighted phantom MR images of [Gd**L3**(H_2O)] chelate at different concentrations were also recorded by using clinical MRI scanners. The increasing quality of the images is correlated to increasing concentrations of complex.

To summarize, in spite of a solubility in water which has yet to be improved, our studies highlight the promising theranostic potential of azamacrocyclic Gd^{3+} complexes combining 2PE-PDT as therapy modality and MRI as imaging technic and paves the way to the synthesis of new “all-in-one” metal-based probes.

Experimental

Starting materials were purchased from Sigma Aldrich, Acros Organics, Alfa Aesar or Chematech with the best available quality grade. All reactions were routinely performed under argon atmosphere in anhydrous solvents when relevant. Column chromatography was performed using Acros Ogranics (0.035-0.70 mm) silica gel or alumina activated with 6% mass of water.

Synthesis

Compounds **1**,[55] **2**,[38] **5**[56] and **10**[52] were synthesised following previously reported procedures. The synthesis of the compounds: **3**, **4, 6**, **7**, **8**, **9**, **11**, [Gd**L2**(H_2O)] and [Gd**L3**(H_2O)] is included in supplementary information. Analytical HPLC was performed on a Prominence Shimadzu HPLC/LCMS-2020 equipped with a UV SPD-20

A detector. The chromatographic system employs HPLC (Vision HT C18 HL 5 µ 250× 4.6 mm) with H_2O and MeCN as eluents at a flow rate of 1 mL/min and UV detection at 254 and 350 nm. NMR spectra (^1H, ^{13}C) of **3**-**8** and **9** were recorded at ENS Lyon at room temperature on BRUKER Avance spectrometers operating at 300 MHz or 400 MHz for ^1H and 75 MHz, 101 MHz or 125.7 MHz for ^{13}C NMR spectra were recorded using the µDEFT experiment and signals were assigned using HSQC and HMBC experiments. NMR spectra of **11** were recorded at the "Services communs" of the University of Brest using Bruker DRX 500 (500 MHz), Bruker Avance 500 (500 MHz), Bruker Avance 400 (400 MHz), or Bruker AMX-3 300 (300 MHz) spectrometers at 278K. Chemical shifts are listed in parts per million (δ, ppm) and are reported relatively to residual solvent peaks that are used as internal standards ($CDCl_3$: 7.26 ppm for ^1H and 77.2 ppm for ^{13}C). High resolution mass spectroscopy (HRMS) analyses were performed on a Q-Tof MaXis, sources ESI, APCI, APPI, nano-ESI (at the Institute of Organic and Analytic Chemistry – ICOA in Orléans or at Centre Commun de Spectrométrie de Masse (Villeurbanne, France). All NMR, HR-MS and analytical HPLC spectra are compiled in ESI.

Photophysical measurements

Absorption spectra were recorded on a JASCO V-650 spectrophotometer in diluted solution (ca. 10^{-5} or 10^{-6} mol L^{-1}), using spectrophotometric grade solvents. Emission spectra were measured using Horiba-Jobin–Yvon Fluorolog-3 fluorimeter. The steady-state luminescence was excited by unpolarised light from a 450 W xenon continuous wave (CW) lamp and detected at an angle of 90° for measurements of dilute solutions (10 mm quartz cuvette) by using a Hamamatsu R928. Spectra were corrected for both excitation source light-intensity variation and emission spectral responses. Luminescence quantum yields Q were measured in diluted solutions with an absorbance lower than 0.1, by using the following Equation 1:

$$\frac{\Phi_X}{\Phi_r} = \left[\frac{A_r(\lambda)}{A_r(\lambda)}\right]\left[\frac{n_x^2}{n_r^2}\right]\left[\frac{D_x}{D_r}\right] \quad (1)$$

where A(λ) is the absorbance (or optical density) at the excitation wavelength, n the refractive index of the solvent and D the integrated luminescence intensity. "r" and "x" stand for reference and sample, respectively. Here, the reference is coumarin-153 in methanol (Φ_r = 0.45).[57] Excitations of reference and sample compounds were performed at the same wavelength. The reported results are the average of 4–5 independent measurements at various absorbances (comprised between 0.01–0.1) for both sample and reference. The plot of the integrated luminescence intensity vs. absorbance gives straight line with excellent correlation coefficients and the slope S can be determined for both sample (x) and reference (r). Equation 1 becomes Equation 2.

$$\frac{\Phi_X}{\Phi_r} = \left[\frac{S_X}{S_r}\right]\left[\frac{n_x^2}{n_r^2}\right] \quad (2)$$

For singlet oxygen quantum yield determination ϕ_Δ, the principle is exactly the same except that the singlet oxygen luminescence emission band (D) is integrated for both sample (x) and reference (r) compounds. A(λ) is the absorbance (or optical density) at the excitation wavelength. In this case it is very important that both experiments are conducted in the same solvent at exactly the same excitation wavelength (nx = nr). The reported results are the average of 4–5 independent measurements at various absorbances (comprised between 0.01–0.1) for both sample and reference. The plot of the integrated singlet oxygen luminescence intensity vs. absorbance gives straight line with excellent correlation coefficients and the slope S can be determined for both sample (x) and reference (r). In the present case, the reference is phenalenone ($\phi_{\Delta r}$ = 0.98 in dichloromethane).[58]

The determination of singlet oxygen in water was measured by following the kinetics of dipropionic acid anthracene (DPAA, oxygen scavenger) in the presence or absence of the studied photosensitisers as well as phenalenone used as reference ($\phi_{\Delta r}$ = 0.98 in water) following a previously reported procedure.[59]

Cell biology experiments

Cell culture: MCF-7 human breast cancer cells were purchased in ATCC. They were cultured in Dulbecco's modified Eagle's medium (DMEM) supplemented with 10% fetal bovine serum and 50 µg mL^{-1} gentamycin and maintained in humidified atmosphere at 37°C under 5% CO_2.

Cytotoxic study: MCF-7 cells were seeded into 96-well plates at 2000 cells per well in 200 µL of culture medium and allowed to grow for 24 h. Cells were then incubated for 72 h with increasing concentrations of [Gd**L3**(H_2O)] (0 to 50 µM). As a control, cells were also incubated 72 h with equivalent quantities of DMSO as the Gd^{3+}-complex was dispersed in DMSO. At the end of incubation time, the cells were stained with Hoechst (10 µg mL^{-1}) to highlight nucleus of living cells. Plates were submitted to fluorescent microscope and each well was photographed. Cells were counted and values are reported as mean of 3 experiments ± standard deviations. Control wells were considered as 100% of living cells. The quantity of cell death due to DMSO was removed from the final result to consider only the cell death due to the Gd^{3+}-complex.

PDT experiments*:* for 1P-PDT, cells were seeded into a 384 multi-well plates at 500 cells per well in 50 µL of culture medium and allow to grow for 24 h. Then, cells were incubated 24 h with or without [Gd**L3**(H_2O)] (20 µM). After incubation time, cells were submitted, or not, to light excitation (λ_{exc} ≈ 390 nm, 18 $J.cm^{-2}$, for 10 min) with the mercury lamp of a fluorescence microscope. Finally, 48 h after irradiation, cells were counted using Hoechst staining to evaluate the phototoxicity of the Gd^{3+}-complex.

For 2P-PDT, cells were seeded into a 384 multi-well glass-bottomed plate (thickness 0.17 mm) with a black polystyrene frame at a cell density of 500 cells per well in 50 µL of culture medium, and allowed to grow for 24 h. Then, cells were incubated 24 h with or without [Gd**L3**(H_2O)] (20 µM) and submitted or not to laser irradiation with the Carl Zeiss Microscope (laser power input 3W). Half of the well was irradiated at 800 nm by 3 scans of 1.57 s duration in 4 different areas of the well. The laser beam was focused by a microscope objective lens (Carl Zeiss 10×/0.3 EC Plan-Neofluar). The scan size does not allow irradiating more areas without overlapping. After 2 days, the cell death quantification was performed using Hoechst staining. The value obtained was corrected according to the following formula: Abs [Gd**L3**(H_2O)] No laser – 2 × (Abs [Gd**L3**(H_2O)] No laser – Abs [Gd**L3**(H_2O)] laser).

Relaxivity determination. Measurements of longitudinal (T_1) and transversal (T_2) relaxation times were performed by using a Bruker Minispec MQ-60 NMR Analyzer working at 1.41 T (corresponding to 60 MHz proton Larmor frequency). The temperature of the sample holder was set (25.0 ± 0.2°C) and controlled with the use of a circulating water bath. The T_1 values were determined with the inversion recovery method (180° – τ – 90°) by averaging 4-6 data points obtained at 10 different τ delay values. The transverse relaxation times (T_2) were measured by using the Carr-Purcell-Meiboom-Gill (CPMG) sequence by averaging again 4-6 identical data points. The r_{1p} and r_{2p} relaxivities of the complex [Gd**L3**(H_2O)] complex were determined by using batch samples (lying in the concentration range of 0.087-0.579 mM) by using 32% (v/v%) DMSO/H_2O mixed solvent owing to the solubility problems. The relaxivity of the parent [Gd(**pc2a1pa**)(H_2O)] complex was accessed (using samples prepared in the concentration range of 0.45-1.50 mM)) under the same conditions in order to be able to make direct comparison of the data with those determined for [Gd**L3**(H_2O)]. The pH in the samples containing Gd^{3+} complex was kept constant at pH=7.40 with the use of 50 mM HEPES buffer (*I*=0.15 M NaCl, *T*=298 K). The relaxivity of the $GdCl_3$ was also examined as a function of solvent composition when the DMSO content was varied in the range of 0-30% (v/v%).

MRI imaging. For quantitative MR imaging Siemens Magnetom Essenza 1.5 T (system A) and Philips Achivea 3T (system B) clinical scanners were used. All the MRI scanners were validated. T_1 values were measured with a series of 2D inversion recovery spin-echo (SE) images of varying inversion times (TIs). The acquisition settings for system A were: TIs =100, 200, 300, 400, 500, 600, 700, 800, 900, 1000, 1200, 1400, 1600, 1800, 2000 msec, repetition times (TRs)=3630, 3100, 3060, 3130, 3260, 3410, 3580, 3750, 3930, 4110, 4490, 4870, 5260, 5650, 6040 ms, echo time (TE)=11 msec, acquisition matrix=448×423×20 and image spatial resolution=0.535×0.535×5 mm^3. The settings for system B were: TIs = 200, 300, 400, 600, 800, 1000, 1200, 1400, 1600, 1800, 2000 msec, TR = 3000 ms, echo time (TE) = 15 msec, acquisition matrix=400×226×20 and image spatial resolution=0.449×0.449×4 mm^3.

The T_2 values were measured for system A with 2D multiecho SE imaging sequences using TEs =14.1, 28.2, 42.3, 56.4, 70.5, 84.6, 98.7, 112.8, 126.9, 141.0, 155.1, 169.2, 183.3, 197.4, 211.5, 225.6 msec, repetition time (TR) = 4000 ms, acquisition matrix = 384×336×20 and image spatial resolution = 0.573×0.573×3 mm^3. For system B the settings were the followings: TEs = 20, 40, 60, 80, 100 msec, repetition time (TR) = 3000 ms, acquisition matrix = 256×201×20 and image spatial resolution = 0.532×0.532×2 mm^3. For each T_1 and T_2 measurement the number of signal averages (NEX) were 1. Following the MRI image reconstruction and defining the volume of interests (VOIs), the MR images were evaluated using MATLAB (MathWorks) software.

Conflicts of interest

There are no conflicts to declare.

Acknowledgements

The authors acknowledge the Ministère de l'Enseignement Supérieur et de la Recherche and the Centre National de la Recherche Scientifique. The authors are also grateful to ANR (SADAM ANR-16-CE07-0015-02) for financial support. They also thank the "Service Commun" of NMR facilities of the University of Brest. The authors acknowledge financial support from the Hungarian National Research, Development and Innovation Office (NKFIH K-128201 and 134694projects). The research was also supported in a part by the EU and co-financed by the European Regional Development Fund under the project GINOP-2.3.2-15-2016-00008.

Notes and references

1. A. C. Sedgwick, J. T. Brewster, P. Harvey, D. A. Iovan, G. Smith, X.-P. He, H. Tian, J. L. Sessler and T. D. James, Metal-based imaging agents: progress towards interrogating neurodegenerative disease, *Chem. Soc. Rev.*, 2020, **49**, 2886-2915.
2. S. A. McFarland, A. Mandel, R. Dumoulin-White and G. Gasser, Metal-based photosensitizers for photodynamic therapy: the future of multimodal oncology?, *Curr. Opin. Chem. Biol.*, 2020, **56**, 23-27.
3. X. Liang, X. Li, L. Jing, X. Yue and Z. Dai, Theranostic porphyrin dyad nanoparticles for magnetic resonance imaging guided photodynamic therapy, *Biomaterials*, 2014, **35**, 6379-6388.
4. C. Truillet, F. Lux, J. Moreau, M. Four, L. Sancey, S. Chevreux, G. Boeuf, P. Perriat, C. Frochot, R. Antoine, P. Dugourd, C. Portefaix, C. Hoeffel, M. Barberi-Heyob, C. Terryn, L. van Gulick, G. Lemercier and O. Tillement, Bifunctional polypyridyl-Ru(II) complex grafted onto gadolinium-based nanoparticles for MR-imaging and photodynamic therapy, *Dalton Trans*, 2013, **42**, 12410-12420.
5. S. S. Kelkar and T. M. Reineke, Theranostics: Combining Imaging and Therapy, *Bioconjugate Chem.*, 2011, **22**, 1879-1903.
6. M. Roy Chowdhury, C. Schumann, D. Bhakta-Guha and G. Guha, Cancer nanotheranostics: Strategies, promises and impediments, *Biomedicine & Pharmacotherapy*, 2016, **84**, 291-304.
7. C.-N. Ko, G. Li, C.-H. Leung and D.-L. Ma, Dual function luminescent transition metal complexes for cancer theranostics: The combination of diagnosis and therapy, *Coord. Chem. Rev.*, 2019, **381**, 79-103.
8. S. Lacerda and É. Tóth, Lanthanide Complexes in Molecular Magnetic Resonance Imaging and Theranostics, *ChemMedChem*, 2017, **12**, 883-894.
9. R. Kumar, W. S. Shin, K. Sunwoo, W. Y. Kim, S. Koo, S. Bhuniya and J. S. Kim, Small conjugate-based theranostic agents: an encouraging approach for cancer therapy, *Chem. Soc. Rev.*, 2015, **44**, 6670-6683.
10. L. B. Josefsen and R. W. Boyle, Unique diagnostic and therapeutic roles of porphyrins and phthalocyanines in photodynamic therapy, imaging and theranostics, *Theranostics*, 2012, **2**, 916-966.
11. C. J. Adams and T. J. Meade, Gd(III)–Pt(IV) theranostic contrast agents for tandem MR imaging and chemotherapy, *Chem. Sci.*, 2020, **11**, 2524-2530.
12. J. Schmitt, V. Heitz, A. Sour, F. Bolze, P. Kessler, L. Flamigni, B. Ventura, C. S. Bonnet and É. Tóth, A Theranostic Agent Combining a Two-Photon-Absorbing Photosensitizer for Photodynamic Therapy and a Gadolinium(III) Complex for MRI Detection, *Chem. Eur. J.*, 2016, **22**, 2775-2786.

13. J.-X. Zhang, H. Li, C.-F. Chan, R. Lan, W.-L. Chan, G.-L. Law, W.-K. Wong and K.-L. Wong, A potential water-soluble ytterbium-based porphyrin–cyclen dual bio-probe for Golgi apparatus imaging and photodynamic therapy, *Chem. Commun.*, 2012, **48**, 9646-9648.
14. J. Schmitt, S. Jenni, A. Sour, V. Heitz, F. Bolze, A. Pallier, C. S. Bonnet, É. Tóth and B. Ventura, A Porphyrin Dimer–GdDOTA Conjugate as a Theranostic Agent for One- and Two-Photon Photodynamic Therapy and MRI, *Bioconjugate Chem.*, 2018, **29**, 3726-3738.
15. S. Jenni, F. Bolze, C. S. Bonnet, A. Pallier, A. Sour, É. Tóth, B. Ventura and V. Heitz, Synthesis and In Vitro Studies of a Gd(DOTA)–Porphyrin Conjugate for Combined MRI and Photodynamic Treatment, *Inorg. Chem.*, 2020, **59**, 14389-14398.
16. C. Xie, H.-F. Chau, J.-X. Zhang, S. Tong, L. Jiang, W.-Y. Fok, H.-L. Lung, S. Zha, R. Zou, J. Jiao, C.-F. Ng, P. a. Ma, J. Zhang, J. Lin, K. K. Shiu, J.-C. G. Bünzli, W.-K. Wong, N. J. Long, G.-L. Law and K.-L. Wong, Bladder Cancer Photodynamic Therapeutic Agent with Off-On Magnetic Resonance Imaging Enhancement, *Advanced Therapeutics*, 2019, **2**, 1900068.
17. D. V. Yuzhakova, S. A. Lermontova, I. S. Grigoryev, M. S. Muravieva, A. I. Gavrina, M. V. Shirmanova, I. V. Balalaeva, L. G. Klapshina and E. V. Zagaynova, In vivo multimodal tumor imaging and photodynamic therapy with novel theranostic agents based on the porphyrazine framework-chelated gadolinium (III) cation, *Biochimica et Biophysica Acta (BBA) - General Subjects*, 2017, **1861**, 3120-3130.
18. P. Caravan, J. J. Ellison, T. J. McMurry and R. B. Lauffer, Gadolinium(III) Chelates as MRI Contrast Agents: Structure, Dynamics, and Applications, *Chem. Rev.*, 1999, **99**, 2293-2352.
19. J. Wahsner, E. M. Gale, A. Rodríguez-Rodríguez and P. Caravan, Chemistry of MRI Contrast Agents: Current Challenges and New Frontiers, *Chem. Rev.*, 2019, **119**, 957-1057.
20. M. Magerstädt, O. A. Gansow, M. W. Brechbiel, D. Colcher, L. Baltzer, R. H. Knop, M. E. Girton and M. Naegele, Gd(DOTA): An alternative to Gd(DTPA) as a $T^{1,2}$ relaxation agent for NMR imaging or spectroscopy, *Magnetic Resonance in Medicine*, 1986, **3**, 808-812.
21. A. D. Sherry, P. Caravan and R. E. Lenkinski, Primer on gadolinium chemistry, *Journal of Magnetic Resonance Imaging*, 2009, **30**, 1240-1248.
22. A. Nonat, C. Gateau, P. H. Fries and M. Mazzanti, Lanthanide Complexes of a Picolinate Ligand Derived from 1,4,7-Triazacyclononane with Potential Application in Magnetic Resonance Imaging and Time-Resolved Luminescence Imaging, *Chem. Eur. J.*, 2006, **12**, 7133-7150.
23. A. Nonat, M. Giraud, C. Gateau, P. H. Fries, L. Helm and M. Mazzanti, Gadolinium(III) complexes of 1,4,7-triazacyclononane based picolinate ligands: simultaneous optimization of water exchange kinetics and electronic relaxation, *Dalton Transactions*, 2009, DOI: 10.1039/B907738C, 8033-8046.
24. A. M. Nonat, C. Gateau, P. H. Fries, L. Helm and M. Mazzanti, New Bisaqua Picolinate-Based Gadolinium Complexes as MRI Contrast Agents with Substantial High-Field Relaxivities, *Eur. J. Inorg. Chem.*, 2012, **2012**, 2049-2061.
25. A. Rodríguez-Rodríguez, M. Regueiro-Figueroa, D. Esteban-Gómez, R. Tripier, G. Tircsó, F. K. Kálmán, A. C. Bényei, I. Tóth, A. d. Blas, T. Rodríguez-Blas and C. Platas-Iglesias, Complexation of Ln^{3+} Ions with Cyclam Dipicolinates: A Small Bridge that Makes Huge Differences in Structure, Equilibrium, and Kinetic Properties, *Inorg. Chem.*, 2016, **55**, 2227-2239.
26. W. D. Kim, G. E. Kiefer, F. Maton, K. McMillan, R. N. Muller and A. D. Sherry, Relaxometry, Luminescence Measurement, Electrophoresis, and Animal Biodistribution of Lanthanide(III) Complexes of Some Polyaza Macrocyclic Acetates Containing Pyridine, *Inorg. Chem.*, 1995, **34**, 2233-2243.
27. M. Le Fur, E. Molnar, M. Beyler, O. Fougere, D. Esteban-Gomez, O. Rousseaux, R. Tripier, G. Tircso and C. Platas-Iglesias, Expanding the Family of Pyclen-Based Ligands Bearing Pendant Picolinate Arms for Lanthanide Complexation, *Inorg. Chem.*, 2018, **57**, 6932-6945.
28. M. Le Fur, E. Molnar, M. Beyler, F. K. Kalman, O. Fougere, D. Esteban-Gomez, O. Rousseaux, R. Tripier, G. Tircso and C. Platas-Iglesias, A Coordination Chemistry Approach to Fine-Tune the Physicochemical Parameters of Lanthanide Complexes Relevant to Medical Applications, *Chem. Eur. J.*, 2018, **24**, 3127-3131.
29. A. T. Bui, M. Beyler, Y. Y. Liao, A. Grichine, A. Duperray, J. C. Mulatier, B. L. Guennic, C. Andraud, O. Maury and R. Tripier, Cationic Two-Photon Lanthanide Bioprobes Able to Accumulate in Live Cells, *Inorg. Chem.*, 2016, **55**, 7020-7025.
30. A. T. Bui, M. Beyler, A. Grichine, A. Duperray, J. C. Mulatier, Y. Guyot, C. Andraud, R. Tripier, S. Brasselet and O. Maury, Near infrared two photon imaging using a bright cationic Yb(III) bioprobe spontaneously internalized into live cells, *Chem Commun*, 2017, **53**, 6005-6008.
31. J. Mendy, A. Thy Bui, A. Roux, J. C. Mulatier, D. Curton, A. Duperray, A. Grichine, Y. Guyot, S. Brasselet, F. Riobe, C. Andraud, B. Le Guennic, V. Patinec, P. R. Tripier, M. Beyler and O. Maury, Cationic Biphotonic Lanthanide Luminescent Bioprobes Based on Functionalized Cross-Bridged Cyclam Macrocycles, *Chemphyschem*, 2020, **21**, 1036-1043.
32. A. D'Aléo, A. Bourdolle, S. Brustlein, T. Fauquier, A. Grichine, A. Duperray, P. L. Baldeck, C. Andraud, S. Brasselet and O. Maury, Ytterbium-Based Bioprobes for Near-Infrared Two-Photon Scanning Laser Microscopy Imaging, *Angew. Chem. Int. Ed.*, 2012, **51**, 6622-6625.
33. M. Soulie, F. Latzko, E. Bourrier, V. Placide, S. J. Butler, R. Pal, J. W. Walton, P. L. Baldeck, B. Le Guennic, C. Andraud, J. M. Zwier, L. Lamarque, D. Parker and O. Maury, Comparative analysis of conjugated alkynyl chromophore-triazacyclononane ligands for sensitized emission of europium and terbium, *Chem. Eur. J.*, 2014, **20**, 8636-8646.
34. V. Placide, A. T. Bui, A. Grichine, A. Duperray, D. Pitrat, C. Andraud and O. Maury, Two-photon multiplexing bio-imaging using a combination of Eu- and Tb-bioprobes, *Dalton Trans*, 2015, **44**, 4918-4924.
35. A. T. Bui, A. Roux, A. Grichine, A. Duperray, C. Andraud and O. Maury, Twisted Charge-Transfer Antennae for Ultra-Bright Terbium(III) and Dysprosium(III) Bioprobes, *Chem. Eur. J.*, 2018, **24**, 3408-3412.
36. N. Hamon, M. Galland, M. Le Fur, A. Roux, A. Duperray, A. Grichine, C. Andraud, B. Le Guennic, M. Beyler, O. Maury and R. Tripier, Combining a pyclen framework with conjugated antenna for the design of europium and samarium luminescent bioprobes, *Chem Commun*, 2018, **54**, 6173-6176.
37. N. Hamon, A. Roux, M. Beyler, J. C. Mulatier, C. Andraud, C. Nguyen, M. Maynadier, N. Bettache, A. Duperray, A. Grichine, S. Brasselet, M. Gary-Bobo, O. Maury and R. Tripier, Pyclen-Based Ln(III) Complexes as Highly Luminescent Bioprobes for In Vitro and In Vivo One- and Two-Photon Bioimaging Applications, *J. Am. Chem. Soc.*, 2020, **142**, 10184-10197.
38. M. Galland, T. Le Bahers, A. Banyasz, N. Lascoux, A. Duperray, A. Grichine, R. Tripier, Y. Guyot, M. Maynadier, C. Nguyen, M. Gary-

Bobo, C. Andraud, C. Monnereau and O. Maury, A "Multi-Heavy-Atom" Approach toward Biphotonic Photosensitizers with Improved Singlet-Oxygen Generation Properties, *Chem. Eur. J.*, 2019, **25**, 9026-9034.
39. P. R. Ogilby, Singlet oxygen: there is indeed something new under the sun, *Chem. Soc. Rev.*, 2010, **39**, 3181-3209.
40. Z. Sun, L.-P. Zhang, F. Wu and Y. Zhao, Photosensitizers for Two-Photon Excited Photodynamic Therapy, *Adv. Funct. Mater.*, 2017, **27**.
41. P.-C. Lo, M. S. Rodríguez-Morgade, R. K. Pandey, D. K. P. Ng, T. Torres and F. Dumoulin, The unique features and promises of phthalocyanines as advanced photosensitisers for photodynamic therapy of cancer, *Chem. Soc. Rev.*, 2020, **49**, 1041-1056.
42. G. S. He, L.-S. Tan, Q. Zheng and P. N. Prasad, Multiphoton Absorbing Materials: Molecular Designs, Characterizations, and Applications, *Chem. Rev.*, 2008, **108**, 1245-1330.
43. M. Pawlicki, H. A. Collins, R. G. Denning and H. L. Anderson, Two-photon absorption and the design of two-photon dyes, *Angew. Chem. Int. Ed. Engl.*, 2009, **48**, 3244-3266.
44. S. P. McIlroy, E. Cló, L. Nikolajsen, P. K. Frederiksen, C. B. Nielsen, K. V. Mikkelsen, K. V. Gothelf and P. R. Ogilby, Two-Photon Photosensitized Production of Singlet Oxygen: Sensitizers with Phenylene−Ethynylene-Based Chromophores, *J. Org. Chem.*, 2005, **70**, 1134-1146.
45. T. Gallavardin, M. Maurin, S. Marotte, T. Simon, A. M. Gabudean, Y. Bretonniere, M. Lindgren, F. Lerouge, P. L. Baldeck, O. Stephan, Y. Leverrier, J. Marvel, S. Parola, O. Maury and C. Andraud, Photodynamic therapy and two-photon bio-imaging applications of hydrophobic chromophores through amphiphilic polymer delivery, *Photochem Photobiol Sci*, 2011, **10**, 1216-1225.
46. P. H. Lanoe, T. Gallavardin, A. Dupin, O. Maury, P. L. Baldeck, M. Lindgren, C. Monnereau and C. Andraud, Influence of bromine substitution pattern on the singlet oxygen generation efficiency of two-photon absorbing chromophores, *Org Biomol Chem*, 2012, **10**, 6275-6278.
47. T. Zhang, R. Lan, C. F. Chan, G. L. Law, W. K. Wong and K. L. Wong, In vivo selective cancer-tracking gadolinium eradicator as new-generation photodynamic therapy agent, *Proc Natl Acad Sci U S A*, 2014, **111**, E5492-5497.
48. X. S. Ke, Y. Ning, J. Tang, J. Y. Hu, H. Y. Yin, G. X. Wang, Z. S. Yang, J. Jie, K. Liu, Z. S. Meng, Z. Zhang, H. Su, C. Shu and J. L. Zhang, Gadolinium(III) Porpholactones as Efficient and Robust Singlet Oxygen Photosensitizers, *Chem. Eur. J.*, 2016, **22**, 9676-9686.
49. R. Arppe, N. Kofod, A. K. R. Junker, L. G. Nielsen, E. Dallerba and T. Just Sørensen, Modulation of the Photophysical Properties of 1-Azathioxanthones by Eu^{3+}, Gd^{3+}, Tb^{3+}, and Yb^{3+} Ions in Methanol, *Eur. J. Inorg. Chem.*, 2017, **2017**, 5246-5253.
50. K. R. Johnson and A. de Bettencourt-Dias, 1O2 Generating Luminescent Lanthanide Complexes with 1,8-Naphthalimide-Based Sensitizers, *Inorg. Chem.*, 2019, **58**, 13471-13480.
51. J. X. Zhang, W. L. Chan, C. Xie, Y. Zhou, H. F. Chau, P. Maity, G. T. Harrison, A. Amassian, O. F. Mohammed, P. A. Tanner, W. K. Wong and K. L. Wong, Impressive near-infrared brightness and singlet oxygen generation from strategic lanthanide-porphyrin double-decker complexes in aqueous solution, *Light Sci Appl*, 2019, **8**, 46-56.
52. Z. Garda, E. Molnár, N. Hamon, J. L. Barriada, D. Esteban- Gómez, B. Váradi, V. Nagy, K. Póta, F. K. Kálmán, I. Tóth, N. Lihi, C. Platas-Iglesias. É. Tóth, R. Tripier, G. Tircsó, Complexation of Mn(II) by Rigid Pyclen Diacetates: Equilibrium, Kinetic, Relaxometric, DFT and SOD Activity Studies. *Inorg. Chem. submitted*
53. X. D. Wang and O. S. Wolfbeis, Optical methods for sensing and imaging oxygen: materials, spectroscopies and applications, *Chem. Soc. Rev.*, 2014, **43**, 3666-3761.
54. M. Galland, F. Riobé, J. Ouyang, N. Saleh, F. Pointillart, V. Dorcet, B. Le Guennic, O. Cador, J. Crassous, C. Andraud, C. Monnereau and O. Maury, Helicenic Complexes of Lanthanides: Influence of the f-Element on the Intersystem Crossing Efficiency and Competition between Luminescence and Oxygen Sensitization, *Eur. J. Inorg. Chem.*, 2019, 118-125.
55. A. Picot, C. Feuvrie, C. Barsu, F. Malvolti, B. Le Guennic, H. Le Bozec, C. Andraud, L. Toupet and O. Maury, Synthesis, structures, optical properties, and TD-DFT studies of donor-π-conjugated dipicolinic acid/ester/amide ligands, *Tetrahedron*, 2008, **64**, 399-411.
56. A. Bourdolle, M. Allali, J. C. Mulatier, B. Le Guennic, J. M. Zwier, P. L. Baldeck, J. C. Bunzli, C. Andraud, L. Lamarque and O. Maury, Modulating the photophysical properties of azamacrocyclic europium complexes with charge-transfer antenna chromophores, *Inorg. Chem.*, 2011, **50**, 4987-4999.
57. A. M. Brouwer, Standards for photoluminescence quantum yield measurements in solution (IUPAC Technical Report), *Pure Appl. Chem.*, 2011, **83**, 2213-2228.
58. R. Schmidt, C. Tanielian, R. Dunsbach and C. Wolff, Phenalenone, a universal reference compound for the determination of quantum yields of singlet oxygen O_2 ($^1\Delta_g$) sensitization, *J. Photochem. Photobiol. A: Chem.*, 1994, **79**, 11-17.
59. E. Gandin, Y. Lion and A. Van de Vorst, Quantum yield of singlet oxygen production by xanthene derivatives, *Photochem. Photobiol.*, 1983, **37**, 271-278.